

1986

Propagation of optical waves in tapered fibers and metallic wave guides

Bahram Zandi
Portland State University

Follow this and additional works at: https://pdxscholar.library.pdx.edu/open_access_etds



Part of the [Electrical and Computer Engineering Commons](#)

Let us know how access to this document benefits you.

Recommended Citation

Zandi, Bahram, "Propagation of optical waves in tapered fibers and metallic wave guides" (1986).
Dissertations and Theses. Paper 2693.
<https://doi.org/10.15760/etd.2688>

This Thesis is brought to you for free and open access. It has been accepted for inclusion in Dissertations and Theses by an authorized administrator of PDXScholar. Please contact us if we can make this document more accessible: pdxscholar@pdx.edu.

AN ABSTRACT OF THE THESIS OF Bahram Zandi for the Master of Science in Engineering: Electrical and Computer presented November 25, 1985.

Title: Propagation of Optical Waves in Tapered Fibers and Metallic Wave Guides.

APPROVED BY MEMBERS OF THE THESIS COMMITTEE:

[Redacted Signature]

L. W. Casperson, Chairman

[Redacted Signature]

J. M. Heneghan

[Redacted Signature]

F. Badri

[Redacted Signature]

P. K. Smejtek

The equations for the propagation of Electromagnetic and Optical waves in tapered fibers and metallic waveguides are derived. Solutions are derived for the displacement of the beam from the waveguide axis as a function of distance along the axis, and also for the beam width as a function of distance. These equations are solved numerically for a variety of tapered guides. Experiments are conducted which verify the theoretical results.

PROPAGATION OF OPTICAL WAVES
IN TAPERED FIBERS
AND METALLIC WAVE GUIDES

by

BAHRAM ZANDI

A thesis submitted in partial fulfillment of the
requirements for the degree of

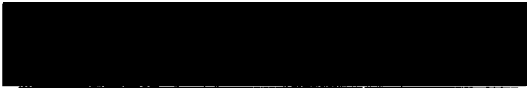
MASTER OF SCIENCE
in
ENGINEERING : ELECTRICAL AND COMPUTER

Portland State University

1986


TO THE OFFICE OF GRADUATE STUDIES AND RESEARCH:

The members of the Committee approve the thesis of
Bahram Zandi presented November 25, 1985.


L. W. Casperson, Chairman


J. M. Heneghan


F. Badi'i


P. K. Smejtek

APPROVED:


Pieter A. Frick, Head, Department of Electrical Engineering


Bernard Ross, Dean of Graduate Studies and Research

TABLE OF CONTENTS

	PAGE
LIST OF TABLES	iv
LIST OF FIGURES	v
CHAPTER	
I. INTRODUCTION	1
II. THEORY	4
a. Derivation of the beam equation	4
b. Solution of the beam equation	7
III. NUMERICAL SOLUTIONS	14
a. Initial Conditions	14
b. Types of Tapers	15
c. Comments on Theoretical data	30
IV. EXPERIMENT	31
A. Procedure	31
B. Results	32
C. Error Analysis	50
V. CONCLUSIONS	51
VI. REFERENCES	52
APPENDICES	56
A. Runge-Kutta methods	56
B. Loss Calculations	60

LIST OF TABLES

TABLE	PAGE
I Pipes and Tapers	17
II Experimental Data	33

LIST OF FIGURES

FIGURE	PAGE
1. Normalized plot of the beam displacement and width along the waveguide	12
2. Geometry of the tapered waveguide	13
3. Beam displacement for $C(1+Gz)$ Taper with $G=0.1$, $C=125.98$ and $2R=5/8$ inch	18
4. Normalized beam width for the previous taper ...	19
5. Beam displacement for $C(1+Gz)$ Taper with $G=0.1$, $C=104.98$ and $2R=3/4$ inch	20
6. Normalized beam width for the previous taper ...	21
7. Beam displacement for $C(1+Gz)$ Taper with $G=0.1$, $C=157.48$ and $2R=1/2$ inch	22
8. Normalized beam width for the previous taper ...	23
9. Beam displacement for $C/(1-Gz)^2$ Taper with $G=0.3$, $C=157.48$ and $2R=1/2$ inch	24
10. Normalized beam width for the previous taper ...	25
11. Beam displacement for $C/(1-Gz)^2$ Taper with $C=104.98$, $2R=3/4$ inch, $G=0.2$ and with $G=0.4$	26
12. Normalized beam width for the previous taper ...	27
13. Beam displacement for $C/(1-Gz)^2$ Taper with $G=0.5$, $C=104.98$ and $2R=3/4$ inch	28
14. Normalized beam width for the previous taper ...	29

LIST OF FIGURES (cont'd):

FIGURE	PAGE
15. The experiment set-up	35
16. Beam propagation along a waveguide	36
17. Schematic drawing of beam propagation along the waveguide	37
18. Experimental graph for Fig. 3	39
19. Experimental graph for Fig. 4	40
20. Experimental graph for Fig. 5	41
21. Experimental graph for Fig. 6	42
22. Experimental graph for Fig. 7	43
23. Experimental graph for Fig. 8	44
24. Experimental graph for Fig. 9	45
25. Experimental graph for Fig. 10	46
26. Experimental graph for Fig. 11	47
27. Experimental graph for Fig. 12	48
28. Experimental graph for Fig. 13	49
29. Attenuation constant	61

CHAPTER I

INTRODUCTION

Long distance optical transmission of voice signals has been the subject of research since the time of Alexander Graham Bell's "Photo-Phone". But the recent discoveries that have revolutionized data transmission do not go back more than two decades. Graded index (lenslike) fibers, trap a light beam because their index of refraction is higher in the core than in the surrounding region. Lenslike media thus constructed were found in 1970 to be the most efficient data transmitters [1]. But for high-power applications and in the frequencies where low-loss fibers are not available metallic waveguides are the only solution. In 1964, Marcatili and Schmeltzer [2], showed that dielectric materials are not suitable for use in hollow circular waveguides for long distance optical transmission because of the high loss due to the slightest curvature of the guide axis. On the other hand they showed that hollow metallic circular waveguides are far less sensitive to curvature of the guide axis, and therefore have less loss. In 1965-66, Kogelnik introduced the ABCD law for the propagation of Gaussian beams of light through lenslike media including those with a loss or gain variation [3-4]. Gaussian light beams in inhomogeneous media were

studied by Casperson in 1973 [5]. A method for determining the width of a beam and its displacement from the axis analytically was introduced; the beam was assumed to have a Gaussian distribution in the transverse direction, and the beam parameter equation was solved exactly. Coupling techniques became a subject of investigation and waveguide tapering was developed. The earliest studies on bent and tapered lenslike media used the ray theory approach [6-10]. In 1976 Sawa [11], dealt with tapered lenslike media from the wave theory point of view. Garmire, et al. [12], showed that when rectangular guides are bent, propagation takes place mainly along the outer walls. Guided beams in concave metallic waveguides were studied by Casperson and Garfield [13]. In that study the beam modes were shown to be expressible in terms of Hermite-Gaussian functions parallel to the strip and Airy functions in the perpendicular direction. They proved an important analogy that along the surface, the equation is similar to that for media with a quadratic index profile (lenslike material), the Hermite-Gaussian solutions of which follow sinusoidal trajectories while oscillating in width. Related studies were done by Marhic et al. [14-15]. Also, polarization and losses of whispering-gallery waves along twisted trajectories was studied by Marhic in 1979 [26]. Analytical and numerical solutions of the beam propagation in tapered quadratic index waveguides have recently been done by Casperson and Kirkwood [16-17]. The purpose of this study is to investigate

theoretically a variety of tapered waveguides and test the theoretical solutions against laboratory experiments.

In order to determine the behavior of light in a tapered waveguide, we assume that a Gaussian beam propagates. This assumption leads to differential equations for the beam width, its radius of curvature, and the displacement of its amplitude center from the longitudinal axis. These equations can then be solved exactly by numerical integration techniques and the results plotted. Therefore the characteristics of the beam and the effects of various forms of tapering are determined exactly in graphical form.

CHAPTER II

THEORY

a. Derivation of the Beam Equation:

To study the behavior of a Gaussian beam propagating along a tapered waveguide, we need to derive a wave equation and therefore we need to start with the four fundamental equations of Electromagnetism known as Maxwell's equations:

$$\nabla \times E = -dB/dt$$

$$\nabla \times H = dD/dt + J$$

$$\nabla \cdot B = 0$$

$$\nabla \cdot D = \rho$$

From the first two equations we get:

$$\begin{aligned} \nabla \times \nabla \times E &= -d/dt (\nabla \times B) = \\ &= -d/dt [\nabla \times (\mu H)] = -d/dt [\nabla \mu \times H - \mu \nabla \times H] \quad (1) \end{aligned}$$

Assuming magnetic homogeneity : $\nabla \mu = 0$ for the permeability

μ . Therefore the equation becomes:

$$\begin{aligned} \nabla \times \nabla \times E &= -\mu d/dt (\nabla \times H) = -\mu d/dt (dD/dt + J) \\ &= -\mu d^2D/dt^2 - \mu dJ/dt \end{aligned}$$

Now substituting:

$$J = \sigma E \text{ (which is true for most materials)}$$

$$\text{and } D = \epsilon_0 E + P \text{ (which is always true) with } P$$

for polarization, we get :

$$-\mu\epsilon_0 d^2E/dt^2 - \mu\sigma dE/dt = -\mu d^2P/dt^2$$

Using the identity:

$$\nabla \times \nabla \times E = \nabla(\nabla \cdot E) - \nabla^2 E$$

and:

$$\nabla(\nabla \cdot E) = -\nabla(E \cdot \nabla \epsilon / \epsilon)$$

we get:

$$-\nabla(E \cdot \nabla \epsilon / \epsilon) - \nabla^2 E = -\mu\epsilon_0 d^2E/dt^2 - \mu d^2P/dt^2 - \mu\sigma dE/dt$$

Now we assume that:

$$\nabla(E \cdot \nabla \epsilon / \epsilon) \ll \nabla^2 E$$

That is, the permittivity ϵ does not change much in a wavelength. Therefore our equation reduces to:

$$\nabla^2 E - \mu\epsilon_0 d^2E/dt^2 - \mu\sigma dE/dt = \mu d^2P/dt^2$$

Analyzing the polarization P into a background component P_0 and a component due to the lasing atoms or ions P_1 we get:

$$P = P_0 + P_1$$

and we can write: $P_0 = \epsilon_0 \chi_0 E$

where $\chi_0 = 1$ is the susceptibility of vacuum. Our equation becomes:

$$\nabla^2 E - \mu\epsilon_0 d^2E/dt^2 - \mu\sigma dE/dt = \mu d^2P/dt^2$$

$$= \mu\epsilon_0 \chi_0 d^2E/dt^2 + \mu d^2P_1/dt^2$$

where

$$\epsilon = \epsilon_0(1 + \chi_0)$$

is the electric permittivity.

Now assuming harmonic time dependence we can write:

$$E = E' \cos wt = \operatorname{Re} E' \exp(iwt)$$

$$P_1 = C \cos wt + S \sin wt =$$

$$= \operatorname{Re} [C \exp(iwt) - iS \exp(iwt)] =$$

$$= \operatorname{Re} (C - iS) \exp(iwt) =$$

$$= \operatorname{Re} P' \exp(iwt)$$

All real parts come out of the equation and our equation becomes:

$$\begin{aligned} \nabla^2 E' + \mu \epsilon \omega^2 E' - i \mu \sigma \omega E' &= \\ &= -\mu \omega^2 C + i \mu \omega^2 S \end{aligned}$$

The real parts have to be equal if the complex parts are equal:

$$C = \epsilon X' E'$$

$$S = \epsilon X'' E'$$

So the equation becomes:

$$\nabla^2 E' + [\mu \epsilon \omega^2 (1 + X') + i \mu \epsilon \omega^2 (X'' - \sigma / \epsilon \omega)] E' = 0$$

or:

$$\nabla^2 E' + k^2 E' = 0 \quad (2)$$

which is sometimes referred to as the Helmholtz equation.

In this equation k is:

$$k = (\mu \epsilon)^{1/2} \omega [(1 + X') + i (X'' - \sigma / \epsilon \omega)]^{1/2}$$

which is the wave number or the propagation constant and is a complex number. If X' , σ and X'' are small, then from the identity:

$$(1 + \epsilon)^{1/2} \cong 1 + \epsilon/2$$

For small ϵ we get:

$$k \cong \omega/c [1 + X'/2 + i/2 (-\sigma / \epsilon \omega + X'')] = \beta + ia$$

with:

$$\rho = w/c (1 + X'/2) ,$$

$$a = w/2c (X'' - \sigma/\epsilon w)$$

where a is the gain or loss coefficient and ρ is the index coefficient.

Equation (2) is the Wave Equation in Optics. It tells us E' once we know k .

b. Solutions of the Beam Equation:

We assume that the beam is uniform in the y direction, polarized in the x direction and propagates parallel to the z axis.

For plane waves equation (2) becomes:

$$d^2E'/dz^2 + k^2E' = 0 \quad (3)$$

For a lenslike material, that is a material whose index of refraction varies quadratically with distance, such as an optical fiber, we can write for the wave number k :

$$k(r,z) = k_0(z) - 1/2k_2(z)r^2$$

$$= \rho + ia$$

k is a complex number that can be separated into real part ρ and imaginary part a :

The real part also can be written as:

$$\rho = 2\pi n/\lambda$$

and it denotes the index of refraction. a denotes loss or gain.

Both a and ρ can be separated as:

$\beta =$

$$\beta_0 - 1/2\beta_2 r^2$$

$a =$

$$a_0 - 1/2a_2 r^2$$

where the subscript 0 denotes index or gain per wavelength. Since the gain or loss per wavelength is always small in practice, a_0 can be neglected.

$$k^2 = k_0^2 - k_0 k_2 r^2 + 1/4 k_2^2 r^4$$

We omit the last term as a postulate or approximation since k does not vary a lot.

In cartesian coordinates:

$$r^2 = x^2 + y^2$$

Here $r = x$ only. To solve equation (3) a useful substitution is :

$$E_x = A(x, z) \exp[-i \int k_0(z) dz] \quad (4)$$

Then equation (3) becomes:

$$d^2 A / dz^2 - 2i k_0 dA / dz - i dk_0 / dz A = 0 \quad (5)$$

We cancel the first term in eq. (5) in what is called the Paraxial Approximation. It assumes that A varies very slowly with z .

To have a Gaussian Beam solution we need to make another substitution:

$$A(x, z) =$$

$$= \exp[-i \{ Q_x(z) x^2 / 2 + S_x(z) x + P(z) \}]$$

Q is the Complex Beam Parameter and it governs the size of the beam and the phase front curvature. S is the Complex

Displacement Parameter and is responsible for the location of the beam and its direction of propagation. P is the Complex Phase Parameter and it is related to the phase and amplitude of the beam. Substituting eq. (6) in eq. (5) and equating the equal powers of the equation we get a set of ordinary differential equations:

$$Q^2 + k_0 dQ/dz + k_0 k_z = 0 \quad (7)$$

$$QS + k_0 dS/dz = 0 \quad (8)$$

$$dP/dz = (-iQ - S^2 - idk_0/dz)/2k_0 \quad (9)$$

Equation (7) is the Beam Parameter Equation and eq. (9) is called the Phase Parameter Equation.

The Kogelnik notation for the Complex Beam Radius ($q = k_0/Q$) is:

$$1/q = Q/k_0 = 1/R - i\lambda/\pi w^2 \quad (10)$$

where R is the radius of curvature of the spherical phase fronts, w is $1/e$ of the amplitude spot-size (width) of the beam, and λ is the wavelength of the medium.

To solve for the path of the beam, we need to change variables in eq. (7) to make it a linear, second order equation. The change of variable would be:

$$Q = 1/x (k_0 dx/dz)$$

Then the eq. becomes:

$$dx^2/dz^2 + k_z/k_0 x = 0$$

which has solutions in terms of Sin and Cos:

$$x = A \cos z (k_z/k_0)^{1/2} + B \sin z (k_z/k_0)^{1/2}$$

Thus the beam width in a lenslike material oscillates sinusoidally about the z axis. The period of oscillation is:

$$\text{Period} = \pi(k_0/k_2)^{1/2}$$

and for real index:

$$\text{Period} = \pi(n_0/n_2)^{1/2} \quad (11)$$

The geometry of the tapered waveguide, as shown in Fig. (1), has transverse radius R and longitudinal radius r .

From the previous papers [13-14], it has been shown the important analogy that the propagation of optical waves along the surface of waveguides are similar to propagation in materials with a quadratic index profile (lenslike materials) such as fibers. They have also shown that the period of oscillation in a concave waveguide in terms of R and r is:

$$\text{Period} = \pi(rR)^{1/2} \quad (11a)$$

By comparing eqs. (11) and (11a) we get:

$$n_2/n_0 = 1/rR \quad (12)$$

Now we change variables in eqs. (7) and (8) as:

$$Q' = Q_{\kappa}/k_0$$

$$S' = S_{\kappa}/k_0$$

and separate Q' and S' into real and imaginary parts:

$$Q' = Q_{r'} + Q_{i'}$$

$$S' = S_{r'} + S_{i'}$$

Therefore equations (7) and (8) turn into:

$$\begin{aligned} dQ_{r'}/dz &= \\ &= Q_{i'}^2 - Q_{r'}^2 - \beta_2/\beta_0 \end{aligned} \quad (13)$$

$$\begin{aligned} dQ_{i'}/dz &= \\ &= -2Q_{r'}Q_{i'} - a_2/\beta_0 \end{aligned} \quad (14)$$

$$\begin{aligned} dS_r' / dz &= \\ &= Q_1' S_1' - Q_r' S_r' \quad (15) \end{aligned}$$

$$\begin{aligned} dS_1' / dz &= \\ &= Q_r' S_1' - Q_1' S_r' \quad (16) \end{aligned}$$

Equations (13-16) are Ricatti non-linear and first order differential equations which can be easily solved on computer using Runge-Kutta methods explained in Appendix A.

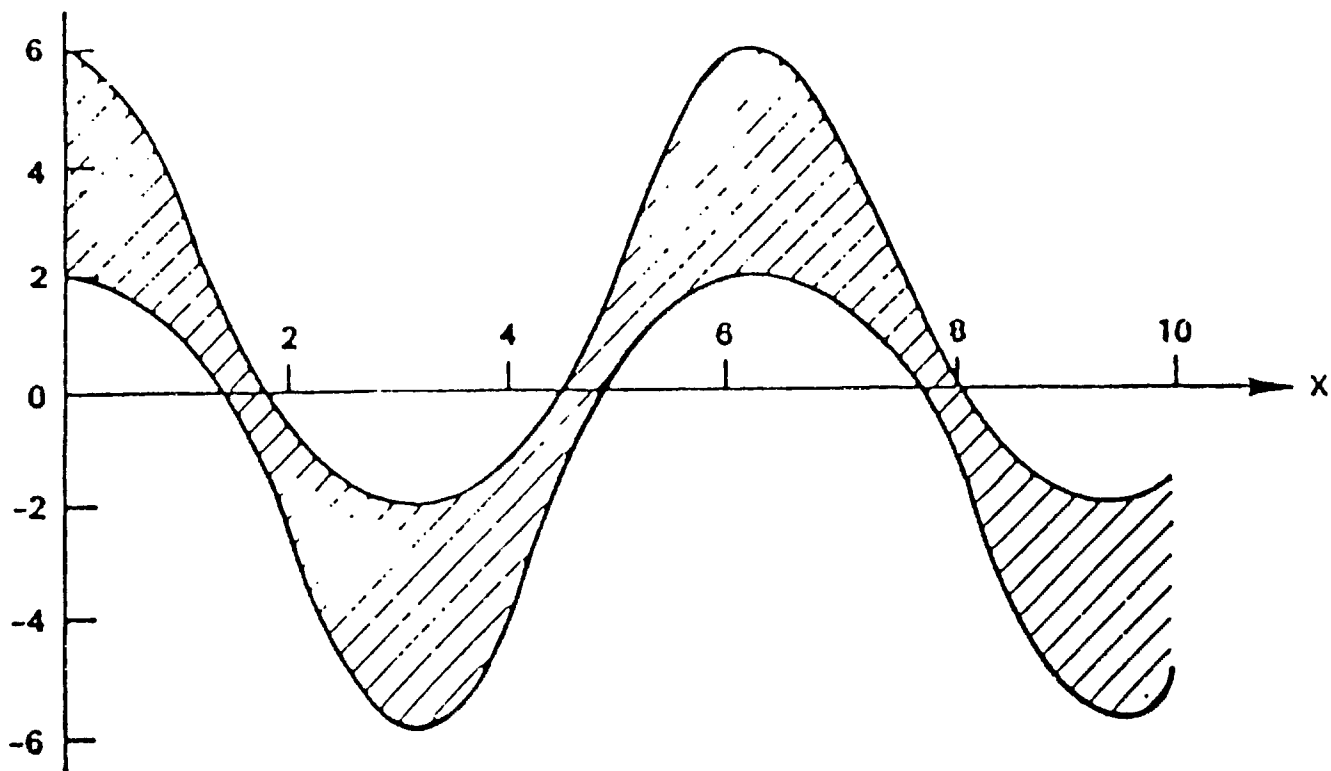


Fig. 1: Normalized plot of the beam displacement and width as a function of distance along the waveguide.

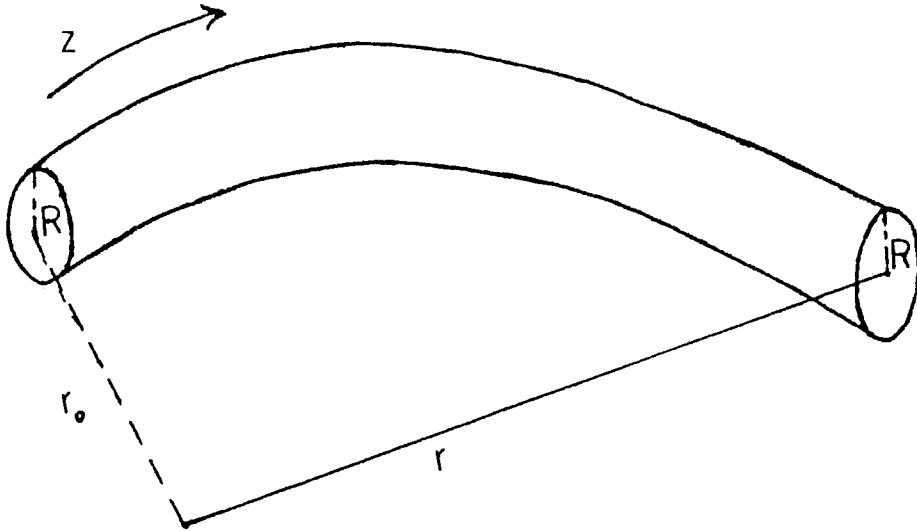


Fig. 2: Geometry of the tapered waveguide.

CHAPTER III

NUMERICAL SOLUTIONS

a. Initial Conditions:

To solve the differential equations (13-16) we need to specify our initial conditions for Qr' , Qi' , Sr' , Si' , ρ_2/ρ_0 , and a_2/ρ_0 which at this point of our study we assume no loss or gain therefore the last term would be equal to zero.

The initial conditions are derived from the steady state beam parameters with no tapering, i.e. zero change with respect to z .

Therefore we set equations (13-16) equal to zero. From eq. (13) we get:

$$\begin{aligned} Qi'^2 - Qr'^2 &= \\ &= \rho_2/\rho_0 \\ &= n_2/n_0 \quad (17) \end{aligned}$$

The amount of eq. (17) is equal to the tapering shown in eq. (12) and which will be discussed later. From eq. (10) in order to have a real spot-size we need to have an imaginary Q' with a negative sign:

$$Qr'(SS) = 0 \quad (18)$$

$$\begin{aligned} Qi'(SS) &= \\ &= -(n_2/n_0)^{1/2} \quad (19) \end{aligned}$$

SS stands for Steady State. From eq. (16) equated to

zero for steady state and with the value of eq. (18) we get:

$$S_r'(SS)=0 \quad (20)$$

From the study [5], the Beam displacement is shown to be:

$$da = -S_i'/Q_i' \quad (21)$$

Therefore:

$$S_i'(SS)=-da(0)Q_i'(SS) \quad (22)$$

where $da(0)$ is the initial beam displacement. We assume this value to be equal to the diameter of the waveguide.

For the tapering we choose different configurations based on early studies [18-21] and initially we assume no loss or gain so that $a_z=0$ in eq. (14).

b. Types of Tapers:

We investigate two types of tapering in eq. (12) which denote the index of refraction:

$$n_z/n_0=1/rR=C(1+Gz) \quad (23)$$

$$\text{and } = C/(1-Gz)^2 \quad (24)$$

where $C=1/r_0R$ when $z=0$ and G is a constant called the Taper Coefficient. Table I shows the different tapers that we have considered and their specifications.

The first set of graphs (Fig. 3-25) show plots of normalized beam width, and amplitude displacement in tapered waveguide versus distance in meters. Values for these quantities are calculated at each step of the integration as follows:

$$w/w(SS) = (Q(SS)/Q_i)^{1/2} \quad (25)$$

$$da = -S_i/Q_i \quad (26)$$

The beam width has been normalized to produce a solution that is independent of wavelength.

TABLE I

Pipes and Tapers

TYPE OF TAPER :

$C(1+Gz)$	with	$G = 0.1$
Pipe one:		$2R = 5/8$ inch
		$C = 125.98$
Pipe two:		$2R = 3/4$ inch
		$C = 104.98$
Pipe three:		$2R = 1/2$ inch
		$C = 157.48$

TYPE OF TAPER :

$C/(1-Gz)(1-Gz)$		
Pipe four:		$2R = 1/2$ inch
		$C = 157.48$
		$G = 0.3$
Pipe five:		$2R = 3/4$ inch
		$C = 104.98$
		$G = 0.4$
Pipe six:		$2R = 3/4$ inch
		$C = 104.98$
		$G = 0.5$
Pipe seven:		$2R = 3/4$ inch
		$C = 104.98$
		$G = 0.2$

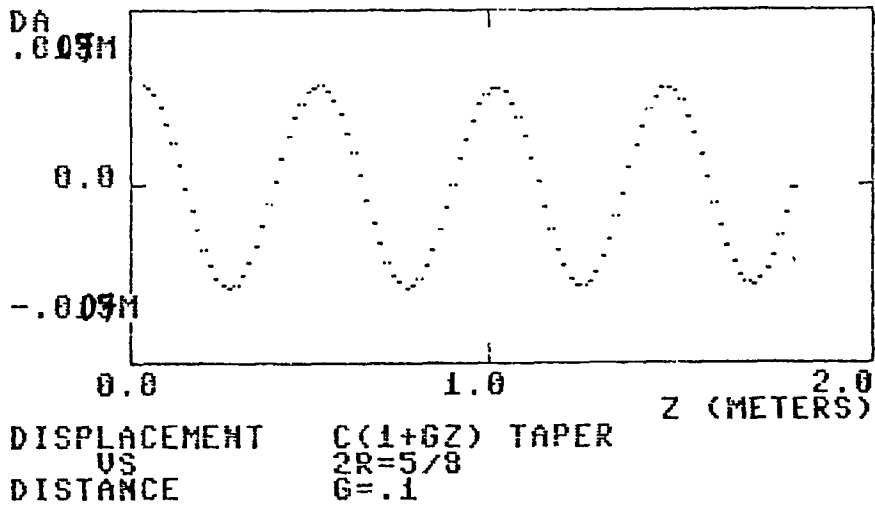


Fig. 3: Beam displacement as a function of distance for $C(1+Gz)$ Taper with $G=0.1$, $C=125.98$ and $2R=5/8$ inch.

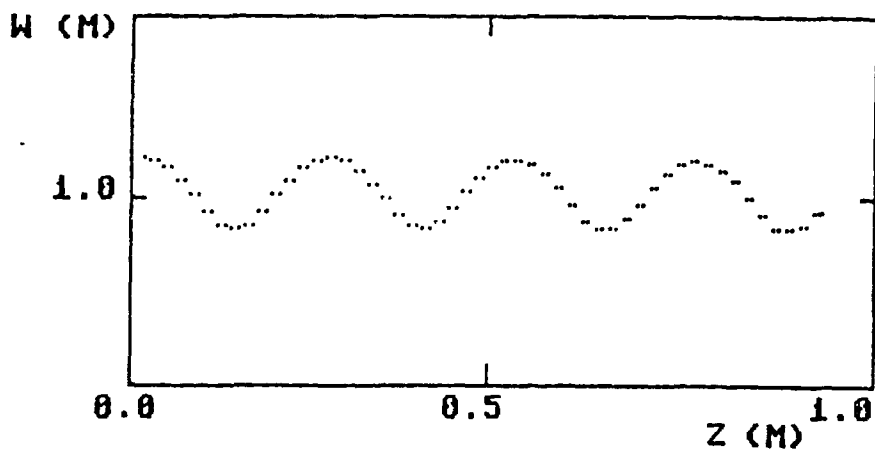
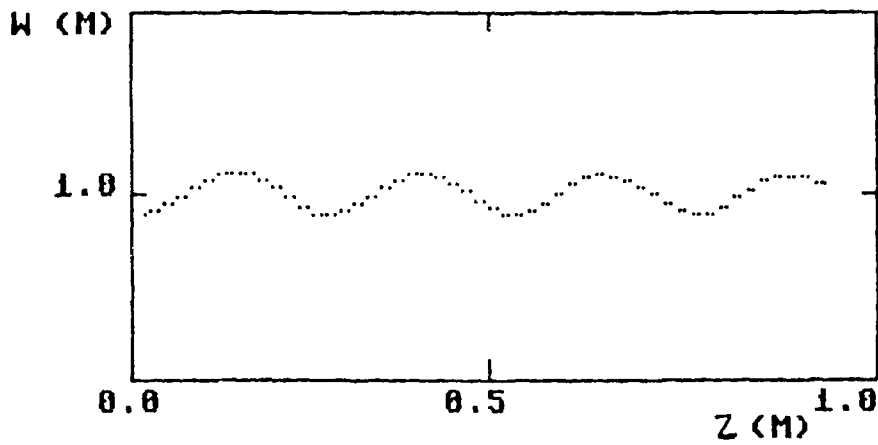


Fig. 4: Normalized beam width as a function of distance for the previous taper with initial spotsize: (top) greater than $w(SS)$, (bottom) less than $w(SS)$.

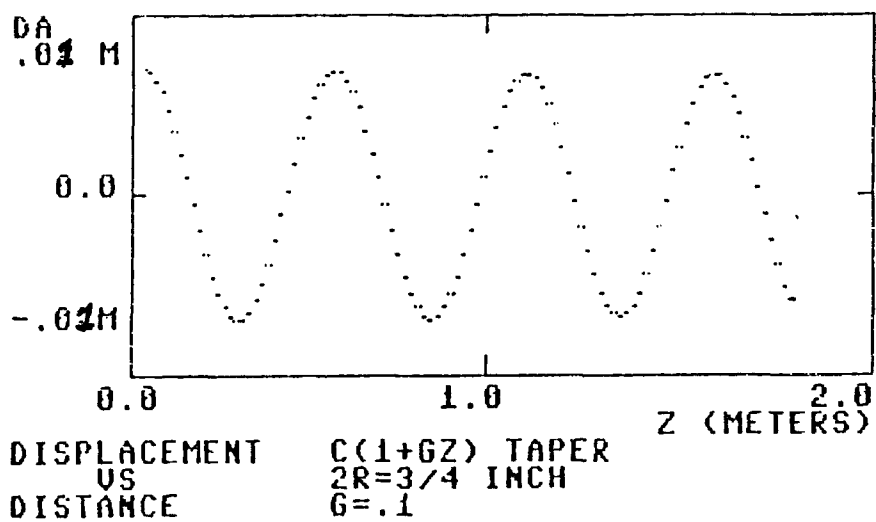


Fig. 5: Beam displacement as a function of distance for $C(1+Gz)$ Taper with $G=0.1$, $C=104.98$ and $2R=3/4$ inch.

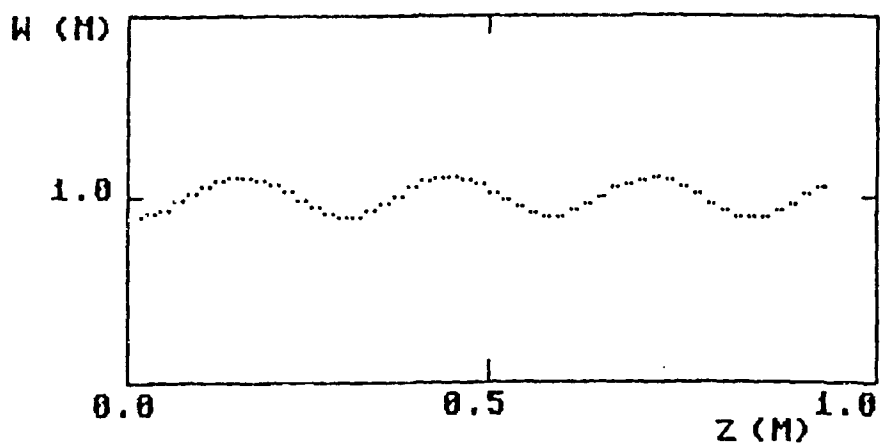
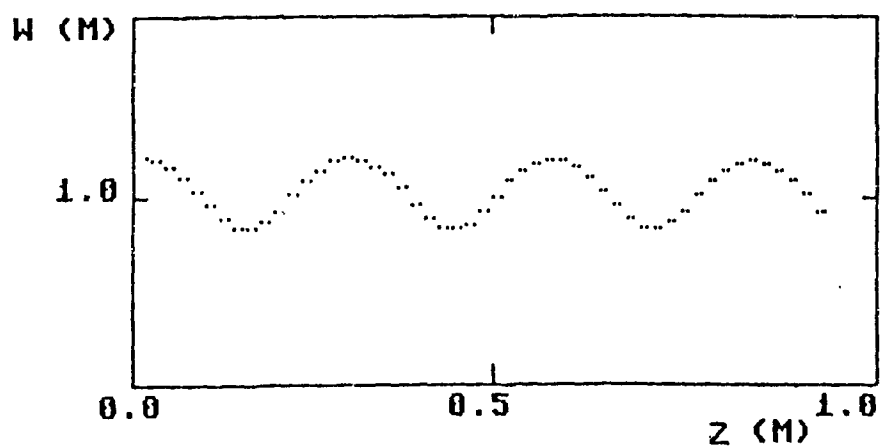


Fig. 6: Normalized beam width as a function of distance for the previous taper with initial spotsize: (top) greater than $w(SS)$, (bottom) less than $w(SS)$.

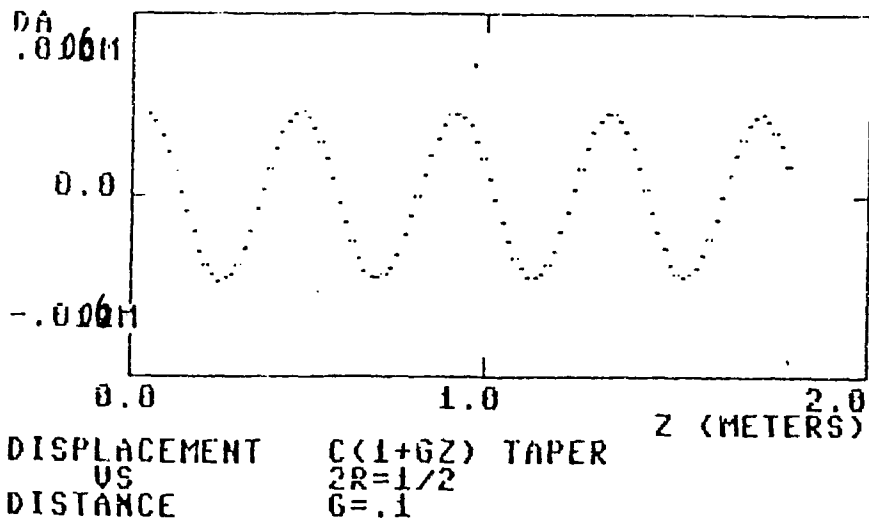


Fig. 7: Beam displacement as a function of distance for $C(1+Gz)$ Taper with $G=0.1$, $C=157.48$ and $2R=1/2$ inch.

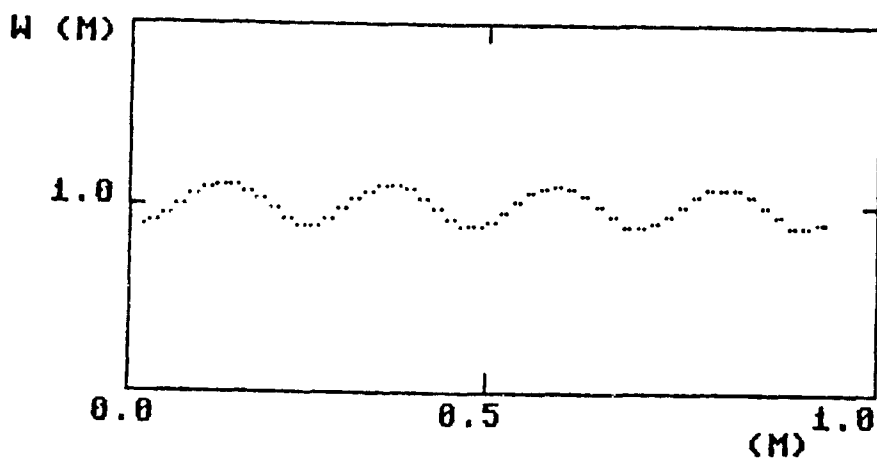
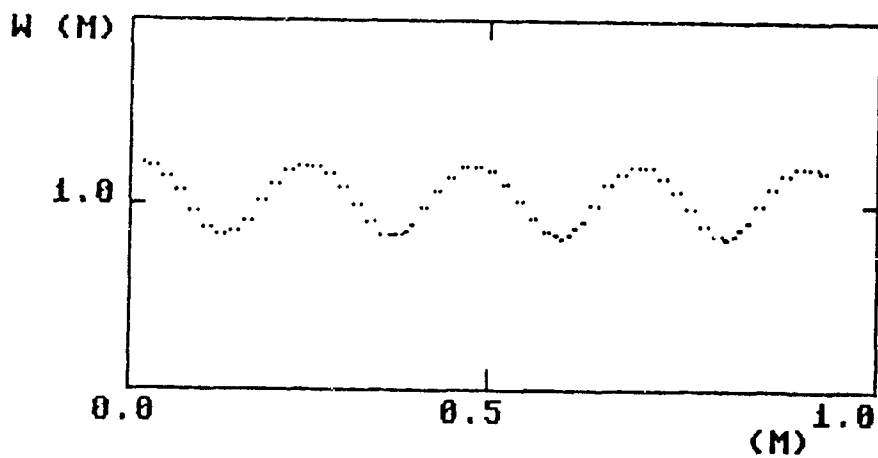


Fig. 8: Normalized beam width as a function of distance for the previous taper with initial spotsize: (top) greater than $w(SS)$, (bottom) less than $w(SS)$.

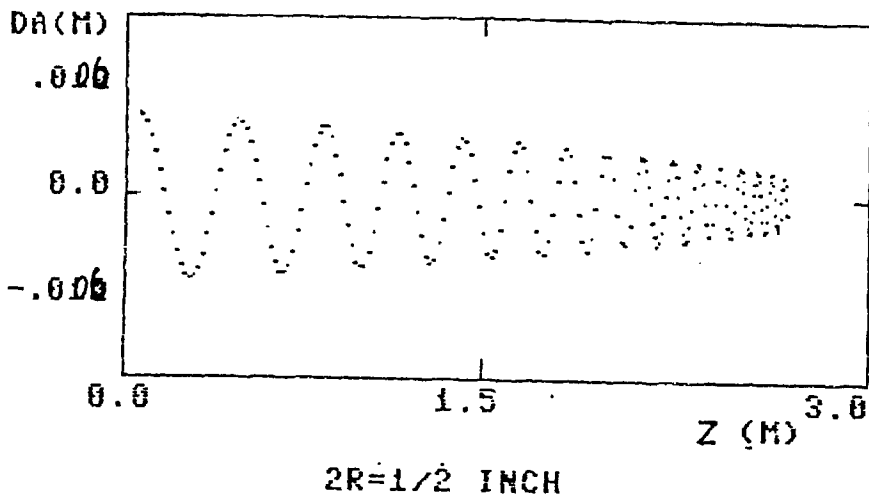


Fig. 9: Beam displacement as a function of distance for $C/(1-Gz)^2$ Taper with $G=0.3$, $C=157.48$ and $2R=1/2$ inch.

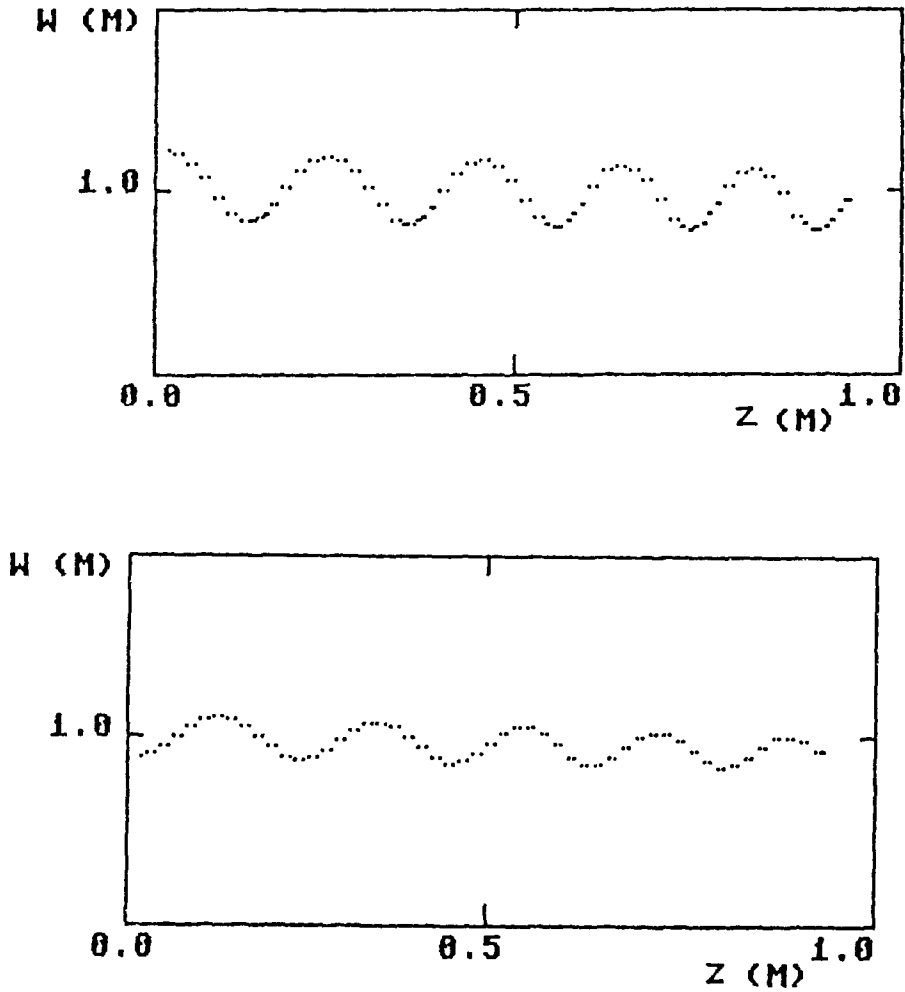


Fig. 10: Normalized beam width as a function of distance for the previous taper with initial spotsize: (top) greater than $w(SS)$, (bottom) less than $w(SS)$.

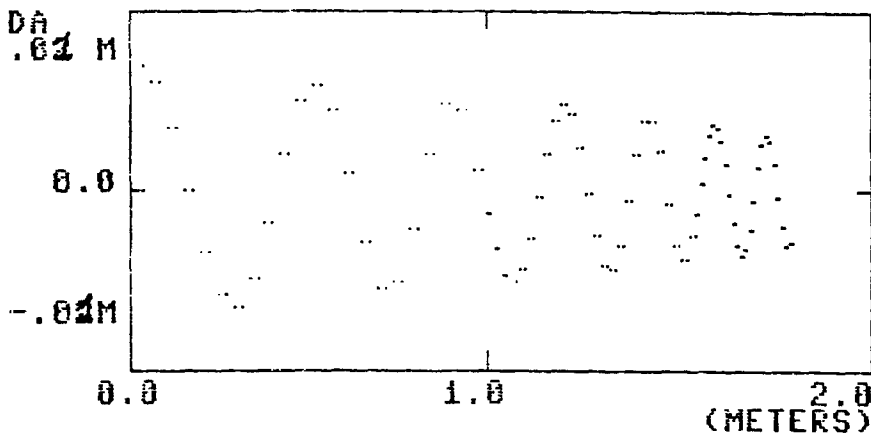
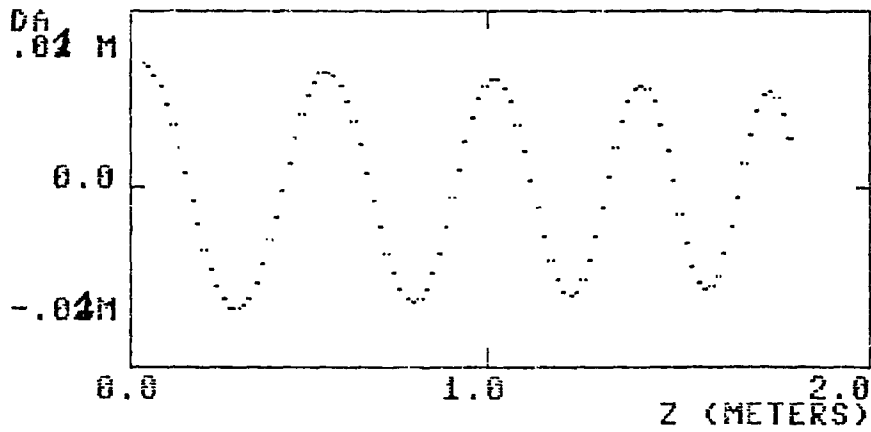


Fig. 11: Beam displacement as a function of distance for $C/(1-Gz)^2$ Taper with $G=0.2$, $C=104.98$ and $2R=3/4$ inch (top) and with $G=0.4$ (bottom).

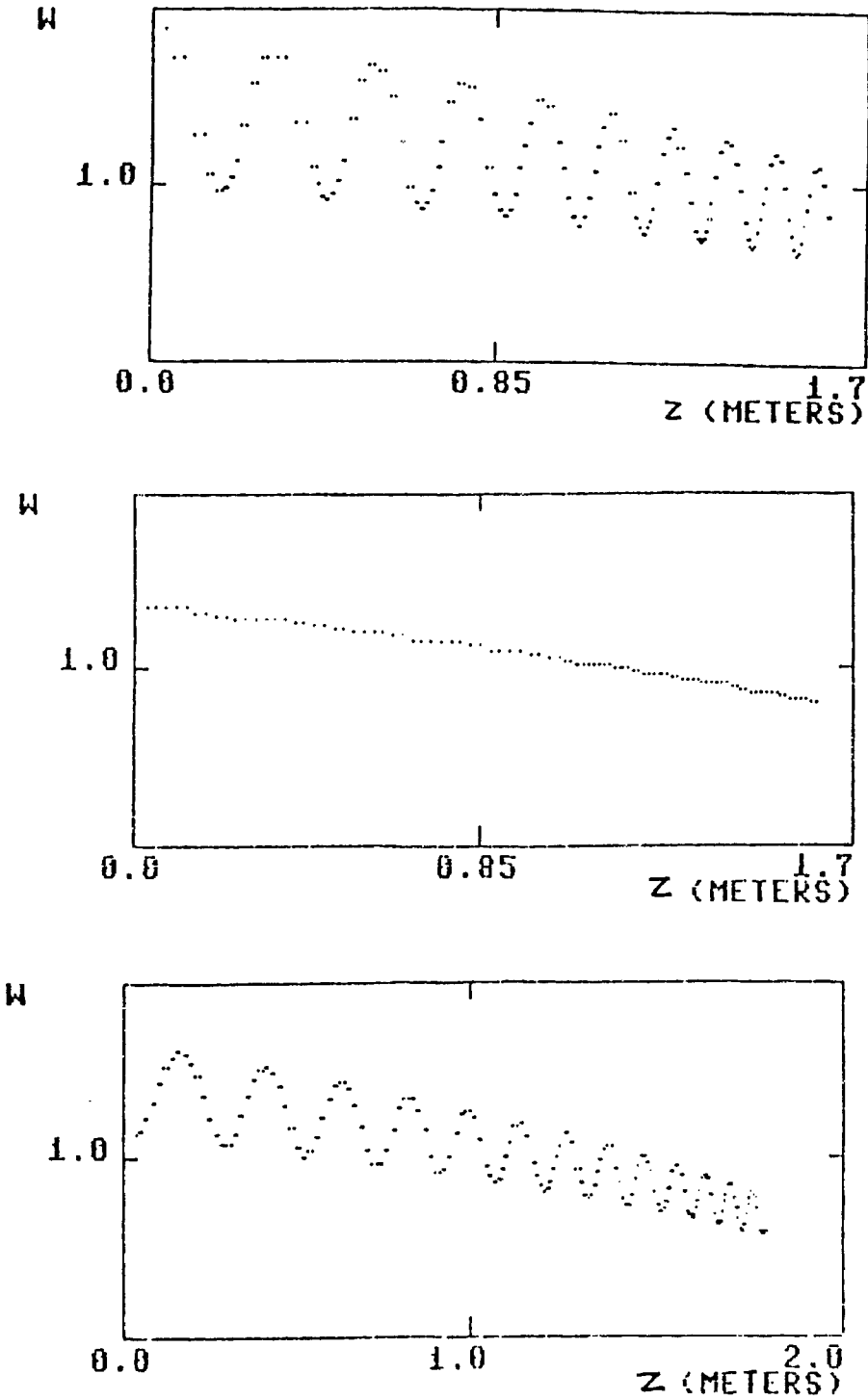


Fig. 12: Normalized beam width as a function of distance for the previous taper with initial spotsize: (top) greater than $w(SS)$, (middle) equal to $w(SS)$, (bottom) less than $w(SS)$.

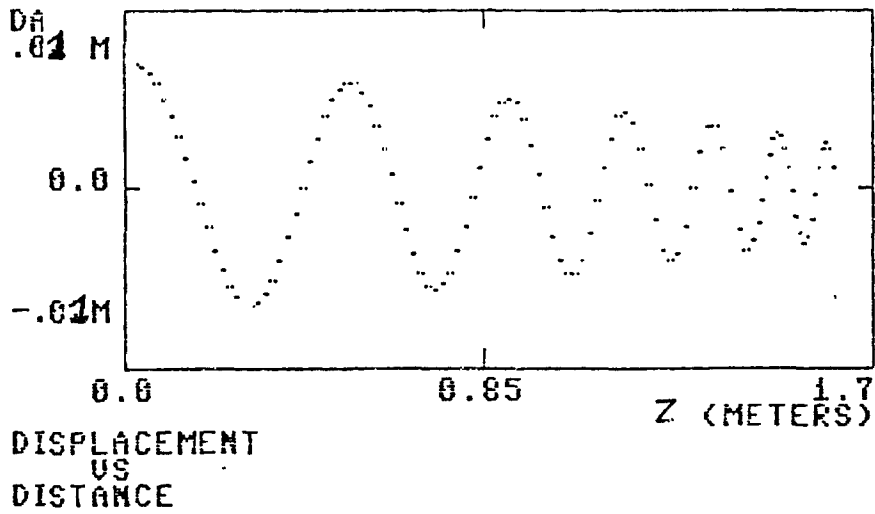


Fig. 13: Beam displacement as a function of distance for $C/(1-Gz)^2$ Taper with $G=0.5$, $C=104.98$ and $2R=3/4$ inch.

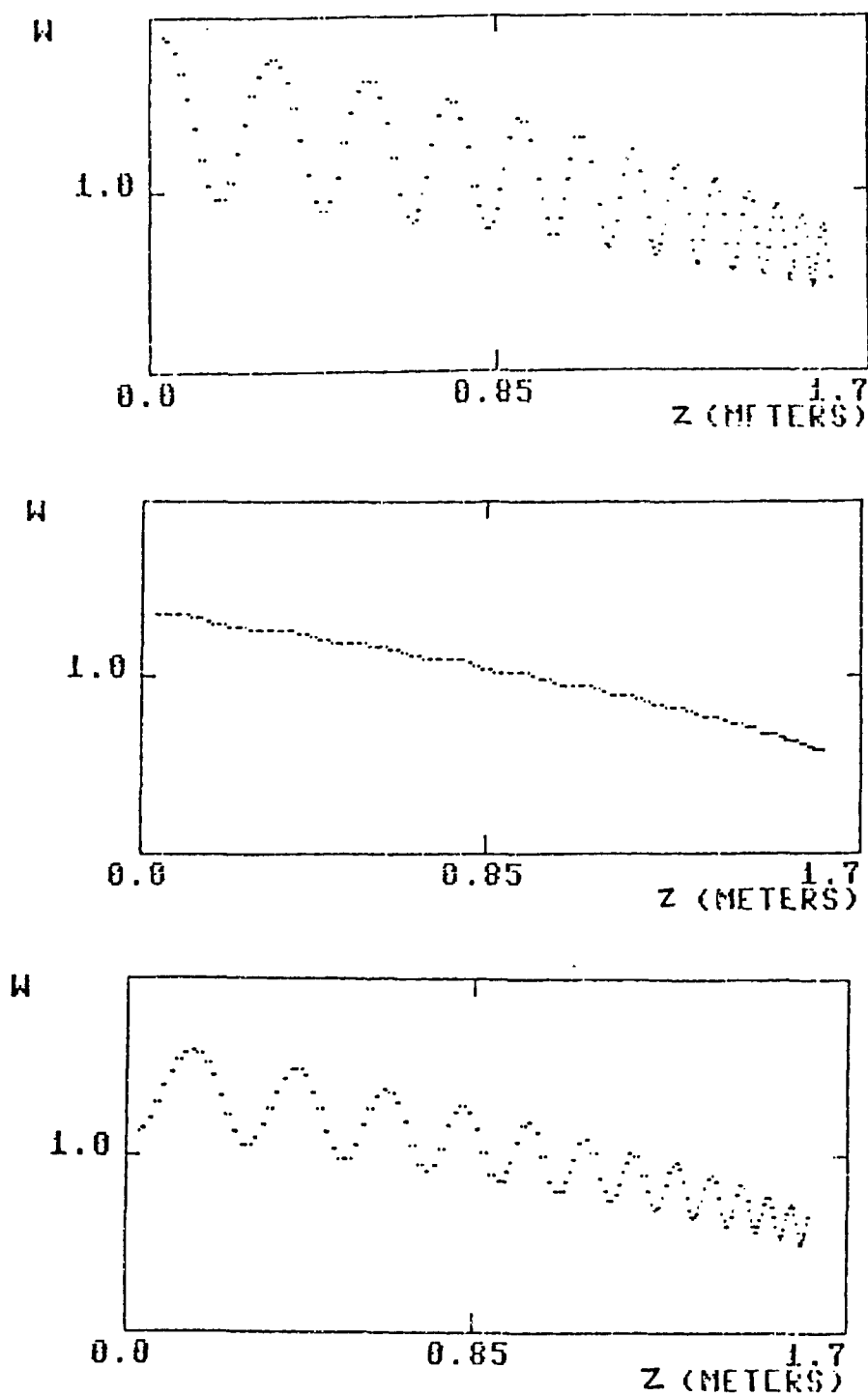


Fig. 14: Normalized beam width as a function of distance for the previous taper with initial spotsize: (top) greater than $w(SS)$, (middle) equal to $w(SS)$, (bottom) less than $w(SS)$.

c. Comments on Theoretical Data:

From the previous graphs for the displacement of the beam, we observe that as the taper becomes sharper (i.e. G approaching 0.5), the oscillation frequency increases whereas the oscillation amplitude (displacement from axis), decreases.

The beam width (spotsizes), however, oscillates about the steady state value when the initial widths are above or below steady state.

CHAPTER IV

EXPERIMENT

A. Procedure:

In order to make a tapered waveguide we needed to find a pipe of a material that could be bent easily and without deformity. This pipe then would be bent according to the tapering formulas of (23) or (24). As is shown in these equations, the tapering does not depend on the type of the material of the waveguide. (The dependence of material is effective in loss calculations as is shown in Appendix B). Copper and Aluminum demonstrated easy bending capability without deformation. Therefore we designed our experiments to be performed with Cu and Al. Different inner radius of the pipes are selected from commercial tubings and the sides of the tubes are chosen to be thick enough to prevent any significant deformation of the transverse radius of curvature due to longitudinal bending. A pipe thus bent is sawed in half and the concave half is selected for the experiment. Then the inside of the waveguide is cleaned and polished using different metal detergents and polishes.

A 6328Å helium-neon laser is positioned at one end of the strip ($z=0$) so that the beam is initially parallel to the longitudinal axis of the strip but displaced from this axis

as far as the strip will allow. The laser beam propagates sinusoidal along the axis of the waveguide strip. We then measure the position of the maxima and minima of the beam displacement from the axis. Due to the loss associated with the metal waveguide, the intensity of the beam is reduced as z increases until the beam is no longer visible, therefore there are limited number of maxima and minima visible. Fig. 15 is a picture of the experiment set up and Fig. 16 is a picture taken from the beam on the waveguide. Fig. 17 is a schematic drawing of what can be observed on the waveguide during the experiment.

B. Results:

Table II gives the measured distance z for the maxima or minima of the beam displacement and spotsize along the different waveguides with different tapering. $2R$ is the pipe diameter, DA is the displacement, and W is the spotsize.

Our actual error has been calculated from:

$$\text{Actual Error} = (\text{Theoretical Value} - \text{Experimental Data}) / \text{Theoretical Value}$$

The Theoretical Error is due to the error in measurements and is the limit for our Actual Error. Those data that exceed this limit have error due to the waveguide fabrication and bending.

TABLE II

Experimental Data

-TYPE OF TAPER: $C(1+Gz)$ with $G=0.1$

2R	z	z	± % ERROR	
inch	EXP. (cm)	THEOR.	THEOR.	EXP.

5/8	35	30	3	16
	57	57	3	0
	77	85	3	9
3/4	23	20	3	15
	55	55	3	0
	85	80	3	6
1/2	25	20	3	25
	50	50	3	0

-TYPE OF TAPER: $C/(1-Gz)(1-Gz)$ with $G=0.3$

1/2	27	27	3	0
	45	45	3	0
	70	70	3	0
	88	85	3	3

- with $G=0.4$

3/4	33	30	3	10
	61	55	3	11
	86	85	3	1
	109	109	3	0

TABLE II (cont'd):

- with $G=0.5$

3/4	54	55	3	1
	92	92	3	0
	112	112	3	0
	128	128	3	0
	143	141	3	1

- with $G=0.2$

3/4	27	27	3	0
	50	62	3	19
	72	72	3	0

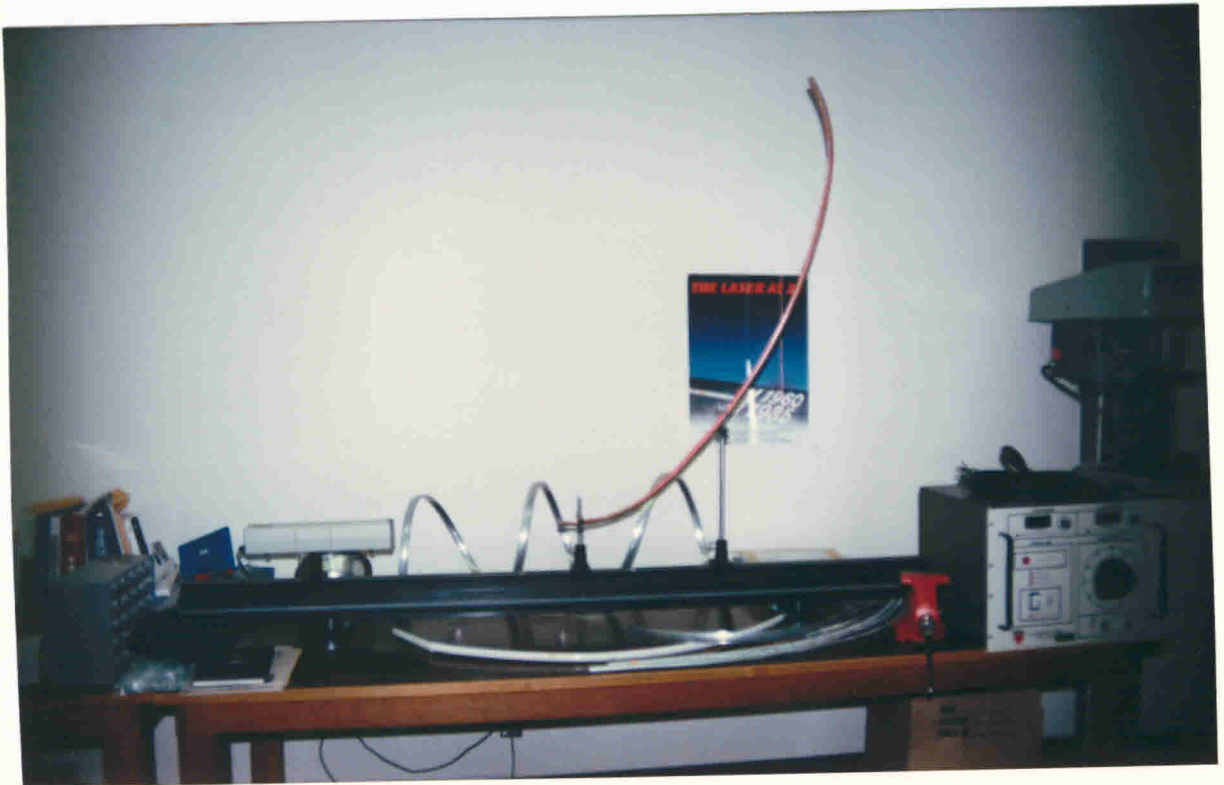


Fig. 15: This picture shows the experiment set-up in the laboratory. A He-Ne laser beam enters a waveguide from the left.

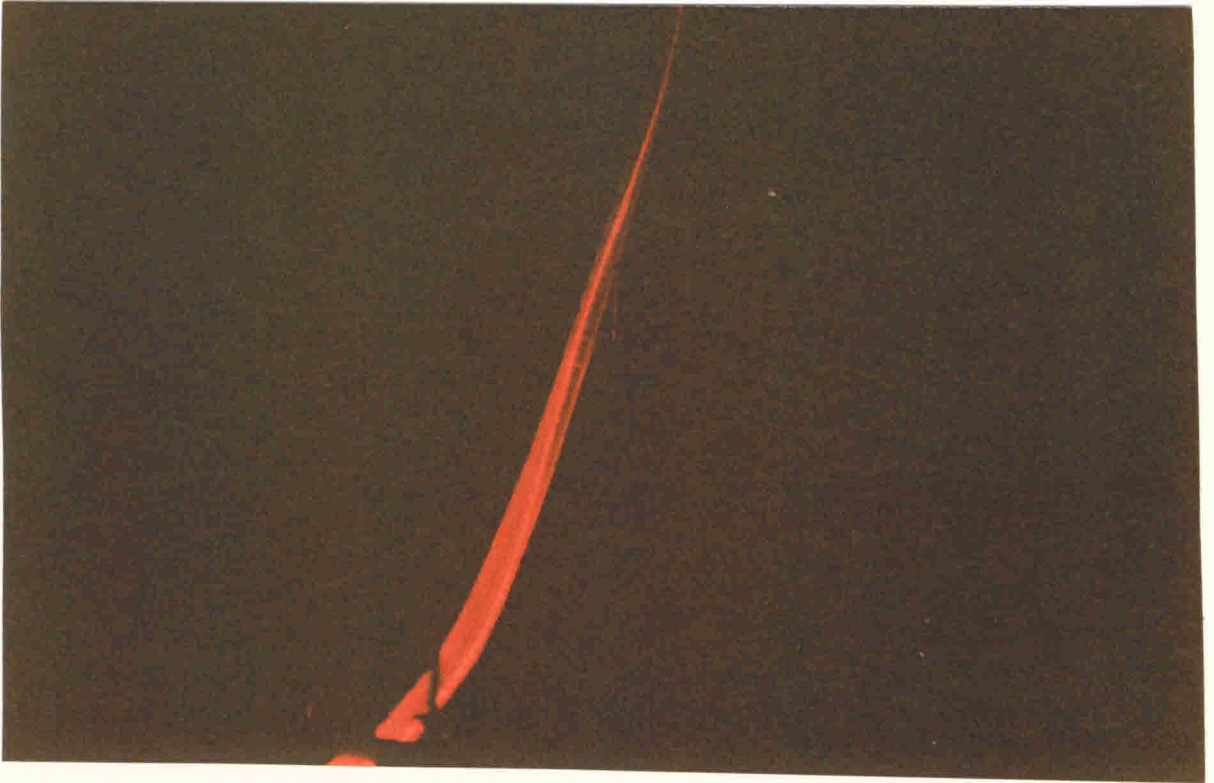


Fig. 16: This picture, taken in the laboratory, shows the beam propagation along a waveguide.

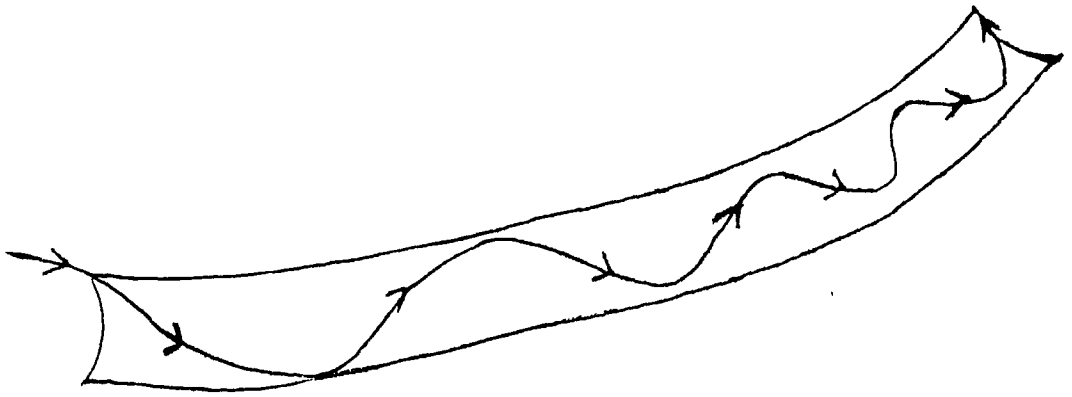


Fig. 17: Schematic drawing of what can be seen along the waveguide. As the taper becomes sharper, the beam displacement gets closer to the axis.

We now superimpose the measured data on the numerical solutions of each taper in the next set of graphs. It can be observed that the theoretical solutions agree closely with experimental data.

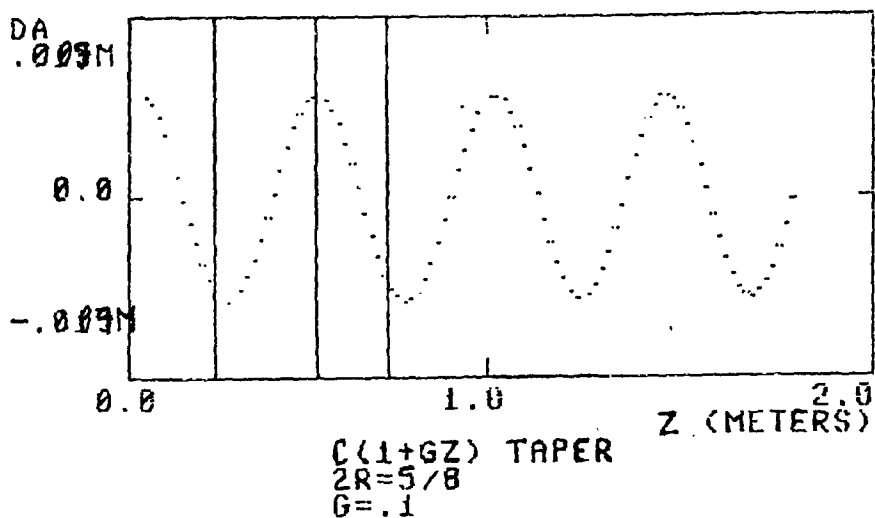


Fig. 10: Experimental data (solid lines) showing locations of maxima and minima are superimposed over theoretical solution (dotted line) of Fig. 3.

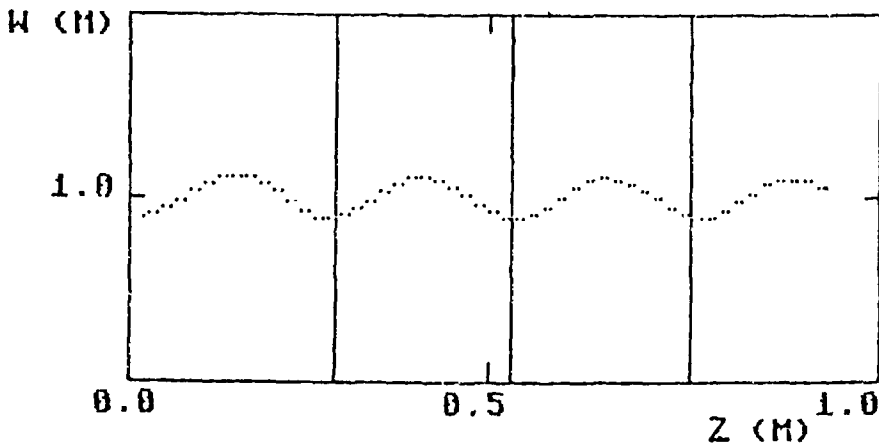
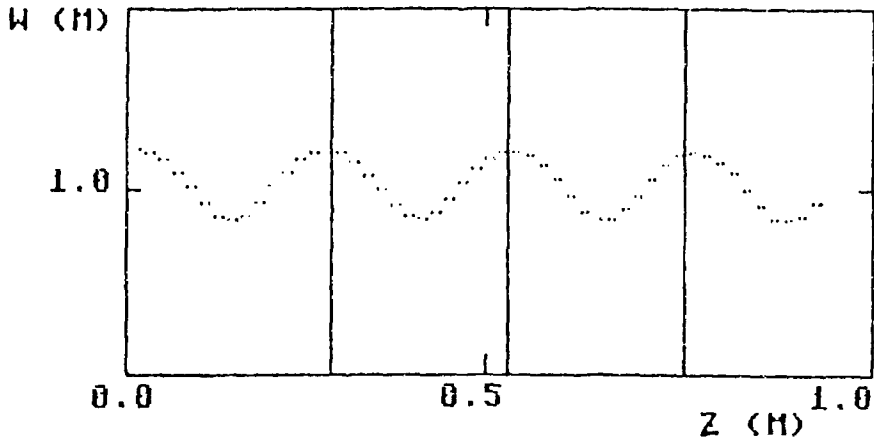


Fig. 19: Experimental data (solid lines) showing locations of maxima and minima are superimposed over theoretical solution (dotted line) of Fig. 4.

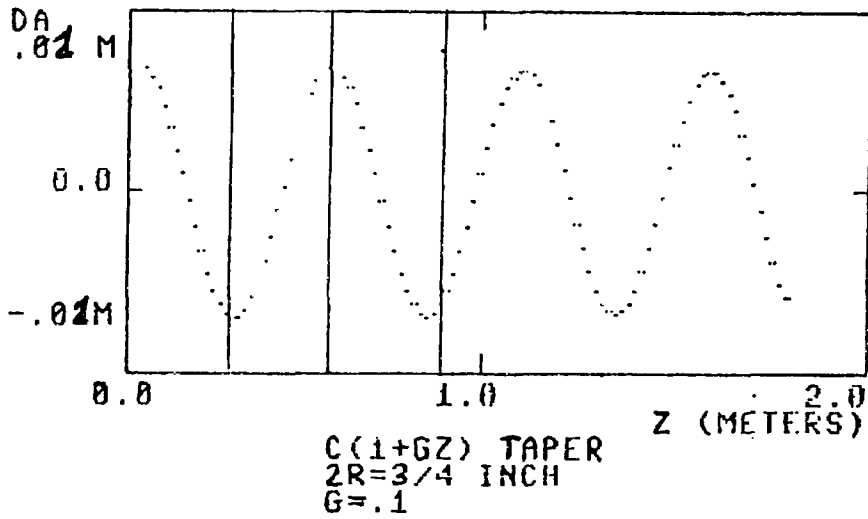


Fig. 20: Experimental data (solid lines) showing locations of maxima and minima are superimposed over theoretical solution (dotted line) of Fig. 5.

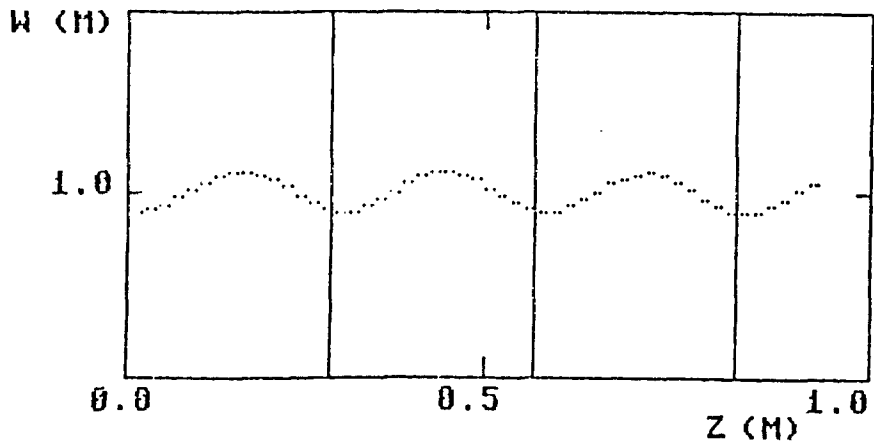
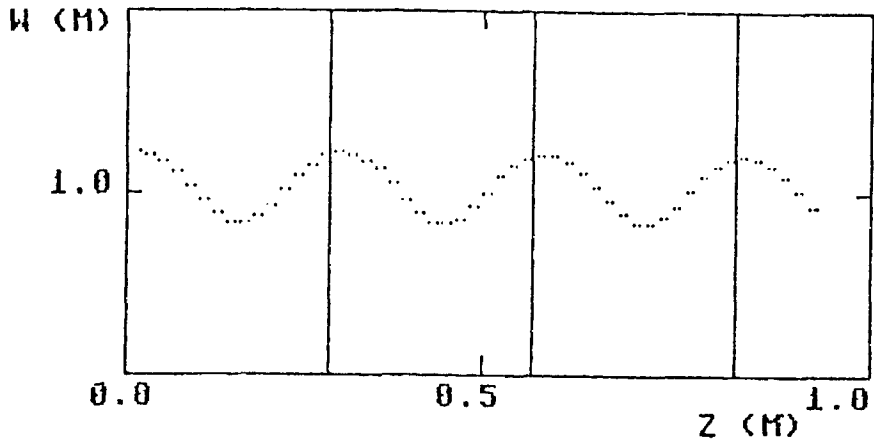


Fig. 21: Experimental data (solid lines) showing locations of maxima and minima are superimposed over theoretical solution (dotted line) of Fig. 6.

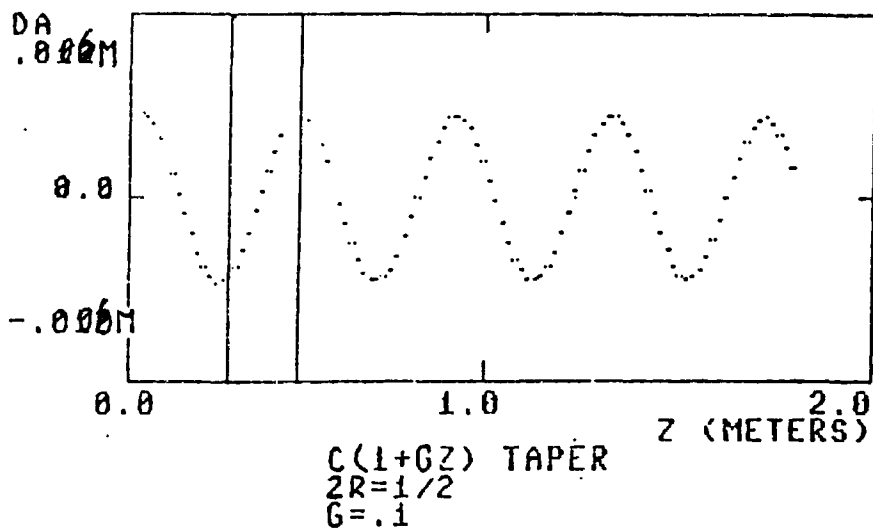


Fig. 22: Experimental data (solid lines) showing locations of maxima and minima are superimposed over theoretical solution (dotted line) of Fig. 7.

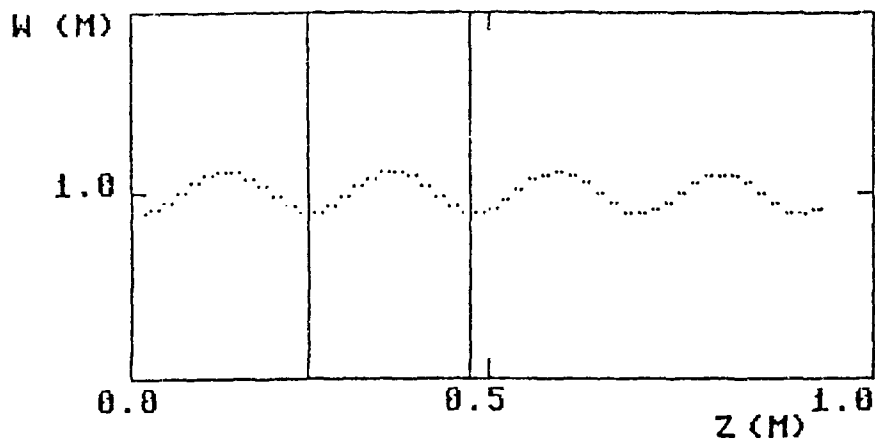
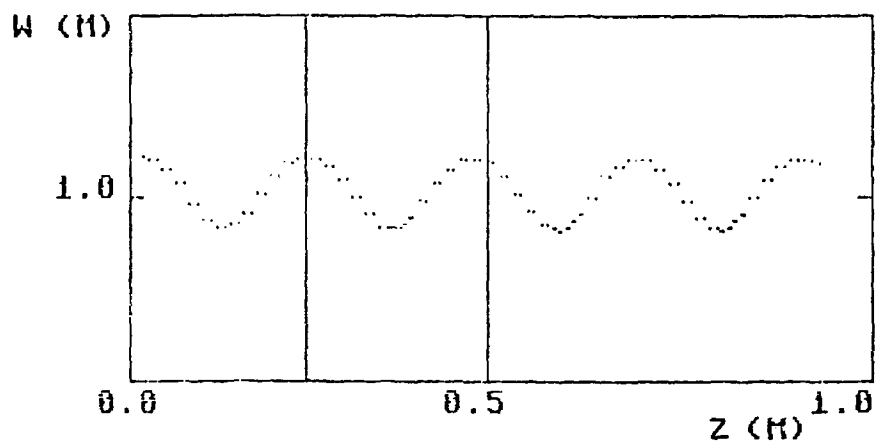


Fig. 23: Experimental data (solid lines) showing locations of maxima and minima are superimposed over theoretical solution (dotted line) of Fig. 8.

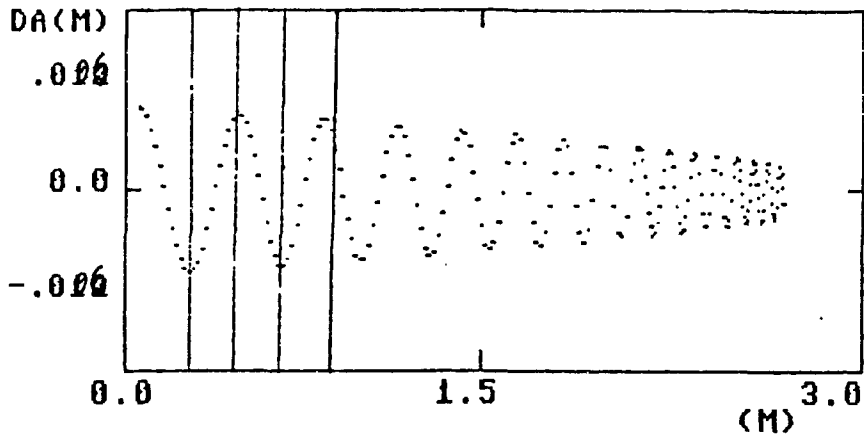


Fig. 24: Experimental data (solid lines) showing locations of maxima and minima are superimposed over theoretical solution (dotted line) of Fig. 9.

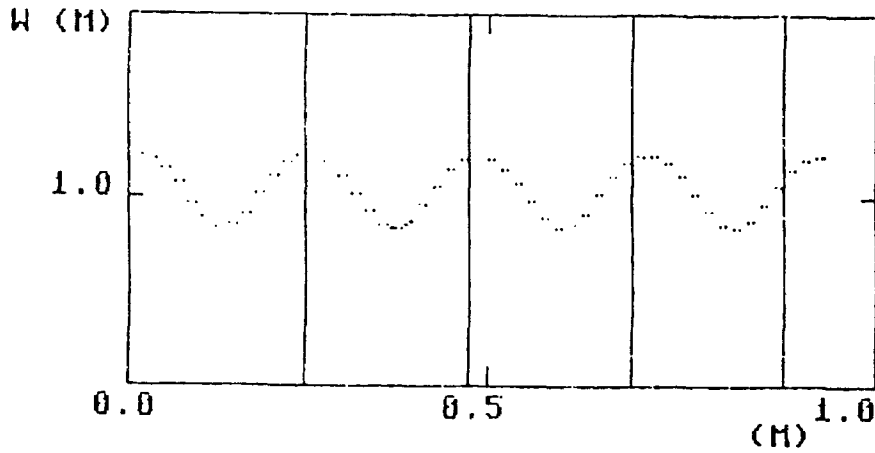
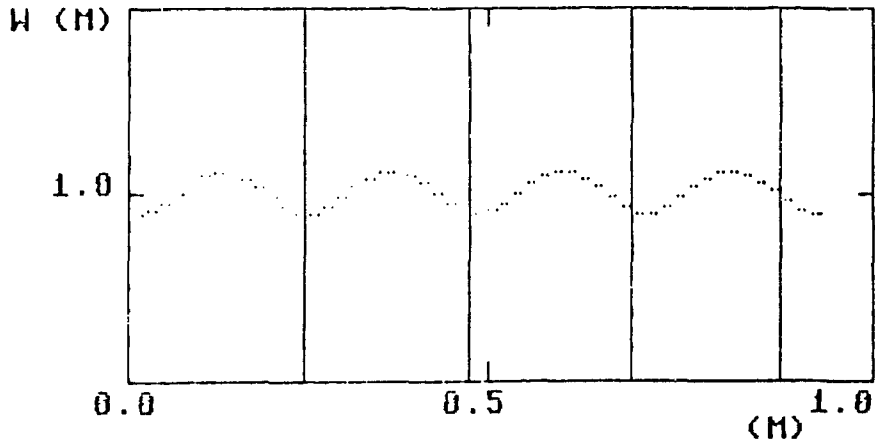


Fig. 25: Experimental data (solid lines) showing locations of maxima and minima are superimposed over theoretical solution (dotted line) of Fig. 10.

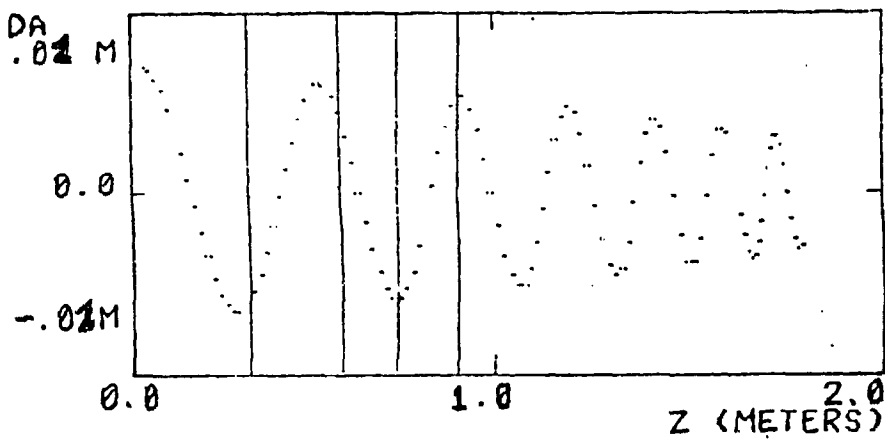
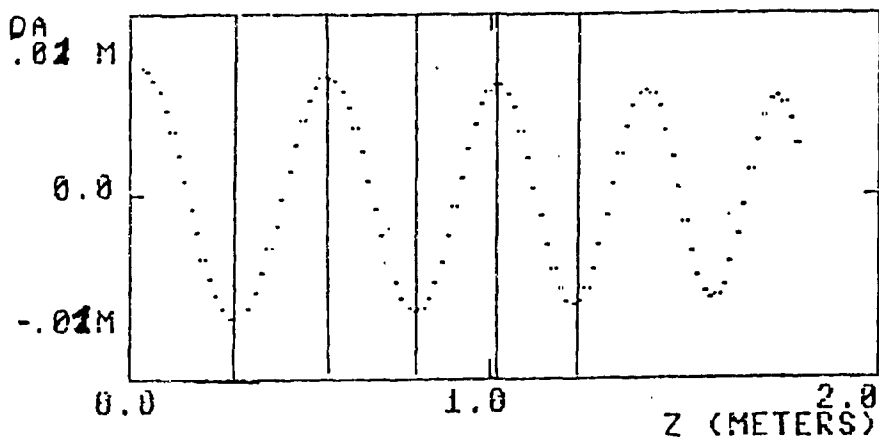


Fig. 26: Experimental data (solid lines) showing locations of maxima and minima are superimposed over theoretical solution (dotted line) of Fig. 11.

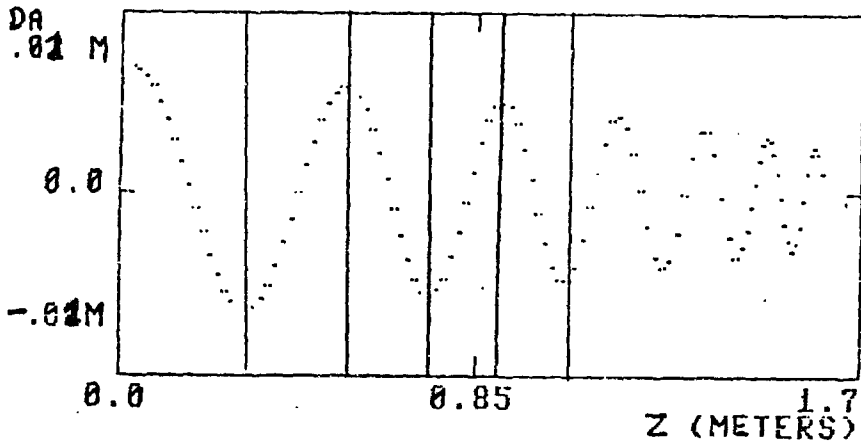


Fig. 27: Experimental data (solid lines) showing locations of maxima and minima are superimposed over theoretical solution (dotted line) of Fig. 13.

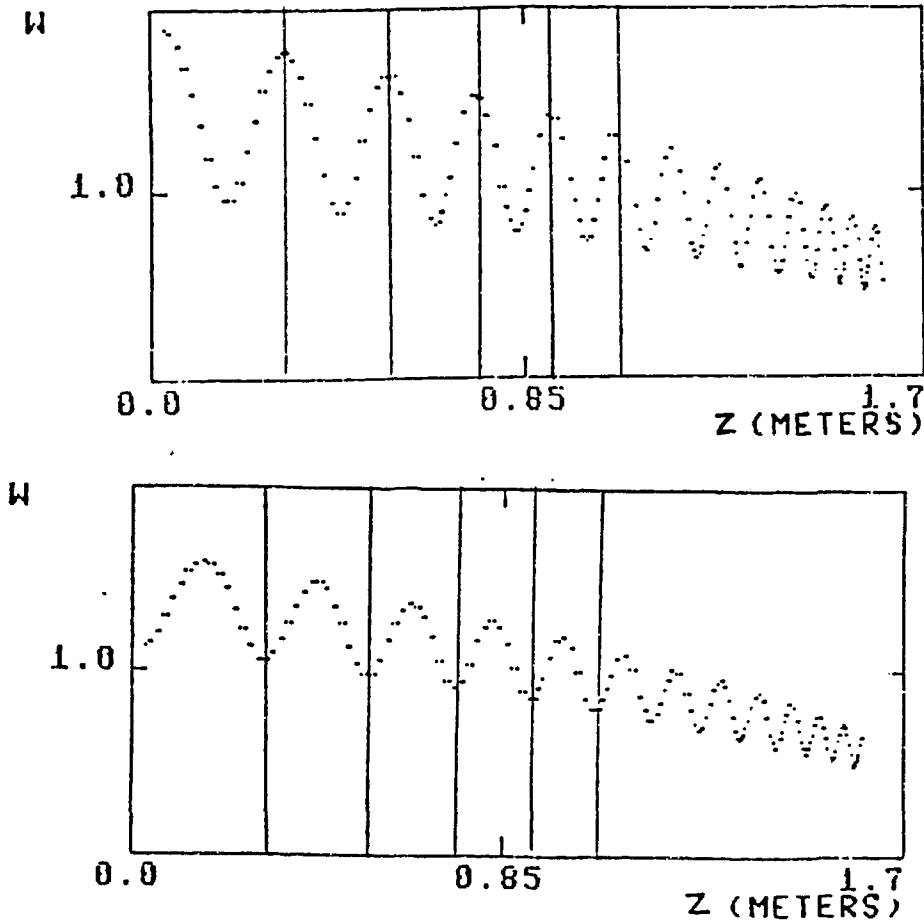


Fig. 28: Experimental data (solid lines) showing locations of maxima and minima are superimposed over theoretical solution (dotted line) of Fig. 14.

C. Error Analysis:

The discrepancies observed between the theoretical values and the experimental data are due to the following errors:

1. The experimental data reading error as calculated in Table II by methods suggested in ref. [25].
2. Propagated error occurred during the experimental set-up.

For the first taper we have:

$$1/rR = C(1+Gz)$$

where R and C and G are constants. r varies with z as we increase z in 0.1 meter intervals. Therefore according to ref. [25] the percentage error can be added and the error for r becomes:

$$\begin{aligned} (\% \text{ error in } r) &= (\% \text{ error in } z) \\ &= \pm 2 \% \end{aligned}$$

For the other taper we have:

$$1/rR = C/(1-Gz)^2$$

Therefore:

$$\begin{aligned} (\% \text{ error in } r) &= 2(\% \text{ error in } z) \\ &= \pm 4 \% \end{aligned}$$

The errors in r transfer back into eq. (13-16) where r relates to the beam parameters and therefore to the beam displacement and width.

3. Error due to the bending of the pipes.

CHAPTER V

CONCLUSIONS

We have obtained exact numerical solutions of the paraxial wave equation. A method for studying the propagation of Gaussian beams in tapered quadratic graded index waveguides is developed. Equations for the beam width (spotsize) and beam displacement as a function of distance have been derived by making assumptions on the initial conditions of the beam. The results from the experiments verified the theory that the beam spotsize and displacement vary sinusoidal. Thus we have verified the analogy between tapered waveguides with quadratic index media.

Obviously the results of this study are limited by our assumptions. First, we have assumed quadratic index for the waveguides and our waves are described by a Gaussian function. Second, we have used the paraxial beam approximation. Therefore we cannot apply the results of this study to cases where these approximations are not valid.

CHAPTER VI

REFERENCES

1. Uchida, T., et al., "Optical Characteristics of a Light-Focusing Fiber Guide and Its Applications," IEEE Journal of Quantum Electronics, Vol. 6, No. 10, October 1970.
2. Marcatili, E. A. J., and Schmeltzer, R. A., "Hollow Metallic and Dielectric Waveguides for Long Distance Optical Transmission and Lasers", The Bell Systems Technical Journal, July 1964, 1783-1809.
3. Kogelnik, H., "On the Propagation of Gaussian Beams of Light Through Lenslike Media Including those with a Loss or Gain Variation," Applied Optics, Vol. 4, No. 12, December 1965.
4. Kogelnik, H., Li, T., "Laser Beams and Resonators," Applied Optics, Vol. 5, No. 10, October 1966.
5. Casperson, L. W., "Gaussian Light Beams in Inhomogeneous Media," Applied Optics, Vol. 12, October 1973.
6. Tien, P. K., Gordon, J. P., and Whinnery, J. R., "Focusing of a light beam of Gaussian field distribution in continuous and periodic lens-like media," Proceedings of IEEE, Vol. 53, Feb. 1965.
7. Suematsu, Y., Kitano, T., "Analysis of a tapered

lens-like media guide," Nat. Conv. Record Inst. Elec. Commun. Eng. Japan., No. 535, 1967.

8. Nishida, K., Nannichi, Y., Uchida T., and Kitano, I., "An avalanche Photodiode with a tapered light-focusing fiber guide", Proc. IEEE (Lett.), Vol. 58, pp. 790-791, May 1970.

9. Yamamoto, S. and Makimoto, T., "Equivalence relations in a class of distributed optical systems-Lens-like media," Applied Optics, Vol. 10, pp. 1160-1163, May 1970.

10. ----, "On the ray transfer matrix of a tapered lenslike medium," Proc. IEEE(Lett.), Vol. 59, pp. 1254-1255, Aug. 1971.

11. Sawa, S., "A Theoretical Study of Light Beams Guided Along Tapered Lenslike Media, and Their Applications", IEEE Trans. of Microwave Theory and Techniques, Vol. MTT-24, No. 2, Feb. 1976.

12. Garmire, E., McMahon, T., and Bass, M., Applied Physics Letters, Vol. 31, No. 92, 1977.

13. Casperson, L. W., Garfield, T. S., "Guided Beams in Concave Metallic Waveguides". IEEE J. of Quantum Electronics, Vol. QE-15, No. 6, June 1979.

14. Marhic, M. E., Kwan, L. I., Epstein, M., "Optical surface waves along a toroidal metallic guide", Appl. Phys. Lett., Vol. 33, No. 7, Oct. 1978.

15. Marhic, M. E., Kwan, L. I., Epstein, M., "Invariant properties of helical-circular metallic waveguides", Appl. Phys. Lett., Vol. 33, No. 10, Nov. 1978.

16. Casperson, L. W. and Kirkwood, J. L., "Beam propagation in tapered index media: numerical solutions", IEEE J. Lightwave Technol., Vol. LT-3, pp. 256-263, April 1985.

17. Casperson, L. W., "Beam propagation in tapered quadratic index media: analytical solutions", IEEE J. Lightwave Technol., Vol. LT-3, pp. 264-272, April 1985.

18. Sodha, M. S., Ghatak, A. K., and Malik, D. P. S., "Electromagnetic wave propagation in radially and axially nonuniform media: geometrical-optics approximation," J. of the Optical Society of America, Vol. 61, pp. 1492-1494, Nov. 1971.

19. Sodha, M. S., Ghatak, A. K., and Malik, D. P. S., "Electromagnetic wave propagation in radially and axially nonuniform media: optics of selfoc fibers and rods: wave optics considerations," J. of Physics D: Applied Physics, Vol. 4, pp. 1887-1892, Dec. 1971.

20. Ghatak, A. K., Malik, D. P. S., Sodha, M. S., "Path of rays in conical selfoc fibers," J. of the Optical Society of America, Vol. 62, pp. 594-595, April 1972.

21. Sharma, A. and Goyal, I. C., "Tapered parabolic-index fiber waveguide," Applied Optics, Vol. 18, pp. 1482-1484, May 1979.

22. Shoup, Terry E., "Applied Numerical Methods for the Microcomputer", Parentice-Hall, Inc., 1984.

23. Krammer, H., "Propagation of modes in curved hollow metallic waveguides for the infrared", Applied Optics,

Vol. 16, No. 8, August 1977.

24. Krammer, H., "Light waves guided by a single curved metallic surface", Applied Optics, Vol. 17, No. 2, Jan. 1978.

25. "Instruction Packet For General Physics Laboratory", Physics Department, Portland State University, Portland, Oregon.

26. Marhic, M. E., "Polarization and losses of whispering-gallery waves along twisted trajectories", J. of Optical Society of America, Vol. 69, No. 9, Sept. 1979.

APPENDICES

A. Runge-Kutta Method with Gill's Modification for a System of Differential Equations[22]:

One-step methods may be used to solve a first-order differential equation of the form:

$$y' = dy/dx = f(x,y) \quad (A1)$$

with initial conditions expressed as y_0 . The purpose of a one-step method is to provide a means for calculating a sequence of y values corresponding to discrete values of the independent variable. The term Runge-Kutta refers to a large family of methods for handling first-order differential equations. The calculation formula for this classical method is:

$$y_{n+1} = y_n + [K(0) + 2K(1) + 2K(2) + K(3)]/6 \quad (A2)$$

where:

$$K(0) = hf(x_n, y_n) \quad (A3)$$

$$K(1) = hf[x_n + 0.5h, y_n + 0.5K(0)] \quad (A4)$$

$$K(2) = hf[x_n + 0.5h, y_n + 0.5K(1)] \quad (A5)$$

$$K(3) = hf[x_n + h, y_n + K(2)] \quad (A6)$$

The most commonly used Runge-Kutta formulation is based on retaining all terms up through h^4 , and therefore it is called "the fourth-order method. In order to achieve optimum efficiency in the computational process, we choose h

to the maximum allowable. Since one can make n first-order differential equations from one n -th order differential equation. As the number of simultaneous equations increases the Runge-Kutta method requires further modifications and it also does not handle the round-off errors. Gill developed a calculation procedure that is well suited for use on the microcomputer because of the following features:

1. It requires a minimum number of storage spaces.
2. It gives the highest attainable accuracy in terms of round-off errors.
3. It requires only a small number of computer instructions to implement.

Gill's procedure applies to a system of $n+1$ first-order equations of the form:

$$y_i'(x) = f_i(x, y_i(x))$$

$$i = 0, 1, 2, \dots, n \quad (A7)$$

Values of y are stored in a two-dimensional array $y_{i,j}$, with the initial conditions as:

$$y_{i,0} = y_i(x_0) \quad \text{for } i = 0, 1, 2, \dots, n$$

$$(A8)$$

For start, a set of coefficients need to be loaded as:

$$a(1) = 1/2$$

$$b(1) = 2$$

$$c(1) = 1/2$$

$$a(2) = 1 - (1/2)^{1/2}$$

$$b(2) = 1$$

$$c(2) = 1 - (1/2)^{1/2}$$

$$a(3)=1+(1/2)^{1/2}$$

$$b(3)=1$$

$$c(3)=1+(1/2)^{1/2}$$

$$a(4)=1/6$$

$$b(4)=2$$

$$c(4)=1/2$$

Register $q_{1,j}$ will be used with:

$$q_{1,0}(x_0)=0, \quad \text{for } i=0,1,\dots,n \quad (\text{A9})$$

First we set the index $j=1$ and then the value of

$$k_{1,j}=f_1(x_{j-1}, y_{0,j-1}, y_{1,j-1}, \dots, y_{n,j-1}) \quad (\text{A10})$$

and

$$y_{1,j}=y_{1,j-1} + [a_j(hk_{1,j} - b_j q_{1,j-1})] \quad (\text{A11})$$

and

$$q_{1,j}=q_{1,j-1} + 3[a_j(hk_{1,j} - b_j q_{1,j-1})] - c_j h k_{1,j} \quad (\text{A12})$$

are calculated for $i=0,1,\dots,n$. Then the procedure from the step k_1 , above is repeated for $j=2,3$, and 4. During the process, the values of x_i are changed as:

$$x_1=x_0+h/2 \quad (\text{A13})$$

$$x_2=x_0+h/2 \quad (\text{A14})$$

$$x_3=x_0+h \quad (\text{A15})$$

After this process we have:

$$y_i(x+h) = y_{i+1}, \quad i=0,1,\dots,n \quad (A16)$$

Now we set:

$$y_{i+1} = y_{i+1} \quad (A17)$$

$$q_{i+1} = q_{i+1} \quad (A18)$$

for $i=0,1,\dots,n$

Then the process starting with the step $j=1$ above is repeated to find subsequent values of y_i .

For accuracy control as the method progresses, the usual procedure is to perform two Gill steps of size h to get:

$$y_i(x+2h) = y_i^{(1)}$$

and then to perform one Gill step of size $2h$ to get:

$$y_i(x+2h) = y_i^{(2)}$$

Since the computation involving the two smaller steps should give greater accuracy, a comparison of these two results at $x+2h$ should provide a measure of the local truncated error. If the difference in the two values is smaller than some prescribed value ϵ , the result is said to be sufficiently accurate. If the difference is larger than the prescribed value, the accuracy can be improved by decreasing the step size by one-half and repeating the process. Therefore the truncation error is

Error =

$$= 1/15 \sum |y_i^{(1)} - y_i^{(2)}| / n+1$$

Thus if $\text{Error} > \epsilon$, then $h = h/2$ and the calculations are repeated to find an answer with more acceptable accuracy prior to going on to the next step. This step-size reduction can be repeated as many times as is

necessary to achieve the desired degree of accuracy.

B. Loss Calculations:

For calculating the losses, we support the study done by Krammer in 1977, [23,24]. In that study, field configurations and attenuation constants of TE-modes in curved parallel-plate metallic waveguides are calculated numerically.

It is assumed that the distance between the plates is much larger than the free space wavelength and that the radius of curvature is much larger than the distance between the plates. The figure below shows attenuation constant of the first TE-modes as a function of curvature. For curvatures not too small the attenuation constant is shown to be inversely proportional to the radius of curvature, but independent of the plate distance:

$$a = 1/R \operatorname{Re}\{1/n\} \quad (B1)$$

where n is the index of refraction of the material of the waveguide.

A plausible explanation for this result is the energy concentration near the outer wall with increasing curvature.

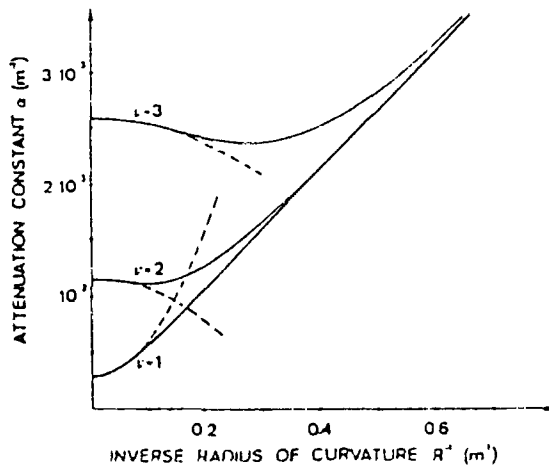


Fig. 29: Attenuation constant α of the first TE modes as a function of curvature ($kd = 600$, $n = 20 - j59$). The mode number is designated by v . The dashed parabolas are the results of a second order perturbation technique.